PCCP

Accepted Manuscript

ROYAL SOCIETY OF CHEMISTRY

www.rsc.org/pccp

Oxidation of $NO^{\bullet}$ by the small oxygen species HO_2^- and $O_2^{\bullet-}$: The role of negative charge, electronic spin and water solvation.

Mauritz Johan Ryding[1], Israel Fernández[2] and Einar Uggerud[1,]*

[1] Mass Spectrometry Laboratory and Centre of Theoretical and Computational Chemistry, Department of Chemistry, University of Oslo, P.O. Box 1033 Blindern, NO-0315 Oslo, Norway,

[2] Departamento de Química Orgánica I, Facultad de Ciencias Químicas, Universidad Complutense de Madrid, 28040-Madrid, Spain.

* einar.uggerud@kjemi.uio.no

Table of contents entry

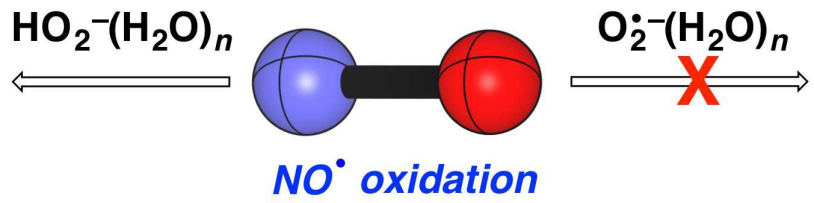

Oxidation of $NO^{\bullet}$ into NO_2^- occurs in reaction with $HO_2^-(H_2O)_n$ clusters but not with $O_2^{\bullet-}(H_2O)_n$ clusters.

Abstract

The reactions of $HO_2^-(H_2O)_n$ and $O_2^{\bullet-}(H_2O)_n$ clusters (n = 0–4) with $NO^{\bullet}$ were studied experimentally using mass spectrometry; the experimental work was supported by quantum chemical computations for the case n = 0, 1. It was found that $HO_2^-(H_2O)_n$ clusters were efficient in oxidizing $NO^{\bullet}$ into NO_2^-; although the reaction rate decreases rapidly with hydration above n = 1. The superoxide–water clusters did not oxidize $NO^{\bullet}$ into NO_2^- under the present experimental

conditions (low pressure); instead a reaction occurred in which peroxynitrite, $ONOO^-$, was formed as a new cluster core ion. The latter reaction was found to need at least one water molecule present on the reactant cluster in order to enable the product to stabilize itself by evaporation of H_2O.

Introduction

$NO^\bullet$ and $NO_2^\bullet$ are spontaneously formed from air gases at high temperatures, as in lightening or in the Birkeland-Eyde process for saltpetre production.[1, 2] Hydrocarbon combustion in air inevitably also leads to the formation of $NO^\bullet$ and $NO_2^\bullet$, so called NO_x.[3] In order to protect local and regional environments it becomes pertinent to remove these unwanted by-products from exhaust gases before they are released into the atmosphere. In densely populated areas increased NO_x concentration leads to health issues, while on larger geographical scales NO_x contributes to acid rain. In automobiles the use of Pt/Rh-based catalysts for exhaust treatment is efficient in reducing NO_x, reforming N_2 and O_2 before the exhaust is released. However, in combustion power plants and in ship engines, low quality fuels (*e.g.* coal and bunker oil) are typically used. Such fuels contain significant amounts of catalyst poisons, which require alternative strategies for NO_x cleaning. Oxidants (*e.g.* H_2O_2)[4-7] or reductants (*e.g.* NH_3)[8] may then be added to convert NO_x to useful or harmless products like saltpetre or N_2. When hydrogen peroxide is used, the reactive species has been identified as the intermediate hydroperoxyl radical $HO_2^\bullet$,[9-11]

$$HO_2^\bullet + NO^\bullet \rightarrow OH^\bullet + NO_2^\bullet \quad (1)$$

The hydroperoxyl radical is then regenerated by reaction of the formed hydroxyl radical with hydrogen peroxide:

$$OH^\bullet + H_2O_2 \rightarrow HO_2^\bullet + H_2O \quad (2)$$

The same reactions are also important in $NO^\bullet$ oxidation in the atmosphere,[12] including thunderstorms where NO_x production is prominent,[13] and even in biology, where $NO^\bullet$ is a well-known blood pressure regulator which is oxidized to $NO_2^\bullet$.[14]

Furthermore, NO_x deposits are directly observed in Corona discharges;[15] more specifically, if ozone and nitrogen oxides are added to the air, or are produced in the discharge in sufficient amounts, NO_3^- ions (including hydrated NO_3^-) are produced and may come to dominate the ion yields.[16-19] These observations indicate that anionic species present in discharges (electrical arc, lightening) may also be involved in $NO^\bullet$ oxidation. Under such conditions it is therefore relevant also to consider the reactivity of $NO^\bullet$ towards likely anionic precursors present in the plasma, like peroxide (HO_2^-) and superoxide ($O_2^{\bullet-}$). Interestingly, these two anions, as well as their water clusters $HO_2^-(H_2O)_n$ and $O_2^{\bullet-}(H_2O)_n$, are formed when pure water is electrosprayed at atmospheric pressure.[20] It is known that $O_2^{\bullet-}$ is able to react with $NO^\bullet$ *in vivo* to form peroxynitrite, $ONOO^-$, in a diffusion controlled reaction.[21] This reaction is probably important in cellular reactions coupled to oxidative stress and $NO^\bullet$ control mechanisms.[22, 23] It has been shown that peroxynitrite can isomerize into nitrate (NO_3^-) in solution, in a reaction that is exothermic by 161 kJ mol^{-1}.[24, 25]

In general, ionic reactions, including ion-molecule reactions, are essential to atmospheric chemistry,[26-29] the significance of atmospheric ions should be emphasised since they also serve as condensation nuclei for water in the atmosphere.[30-32] It is already known that HO_2^- oxidizes NO into NO_2^- in an ion-molecule reaction,[33] and the thermal reaction rate coefficient has been measured.[34]

Here, we report the gas phase reactions of $HO_2^-(H_2O)_n$ and the closely related $O_2^{\bullet-}(H_2O)_n$ (n = 0–4) with $NO^\bullet$. The experimentally observed reactivity was modelled by quantum chemical computations (QCC). The emphasis of our study is on reaction mechanisms, kinetics and thermochemistry. The role of partial hydration is investigated in detail by comparing reactivity as a function of cluster size, n. In addition, we compare the reactivity of the anionic species with that of the corresponding neutrals, *i.e.*, $HO_2^\bullet(H_2O)_n$ and $O_2^\bullet(H_2O)_n$.

Results and discussion

Experimental and computational results for HO_2^- clusters

The experiments were performed using a quadrupole–time-of-flight mass spectrometer (QTOF); the instrument has been described in previous publications.[35-39] The anionic clusters were produced by means of electrospray ionisation. The internal energies of the clusters are low, corresponding roughly to a distribution in the range T = 150–200 K. [35] A single cluster size where selected using a quadrupole mass filter and then transferred into a collision cell where it reacted with $NO^{\bullet}$ before any products and remaining reactants were analysed by time-of-flight. As explained in the Methods Section, there is some uncertainty regarding the absolute $NO^{\bullet}$ pressure in the collision cell and it is estimated to be within 20% of 2.3×10^{-4} mbar; however, reference measurements collected at regular intervals show that while the absolute pressure is uncertain, it is stable over the course of the experiment. Consequently, a corresponding uncertainty (25%) exists in the absolute values of the rate coefficients reported here, while their relative magnitude is expected to be fairly accurate. It should be emphasised here that the reported rate coefficients are given for specific collision energies and are not thermal rate coefficients.

Figure 1 shows the experimental results for $HO_2^-(H_2O)_n$ clusters reacting with $NO^{\bullet}$. The figure shows the rate coefficient for the different types of reaction products observed as a function of the number of H_2O molecules present in the reactant cluster. The data in Figure 1 are given for a centre-of-mass collision energy of 0.6 eV and the reaction channels are integrated over the number of water molecules lost during the reaction (x in Figure 1). The results for $HO_2^-(H_2O)_n$ clusters reacting with $NO^{\bullet}$ at different collision energies can be found in the Supplementary Information Figure S1.

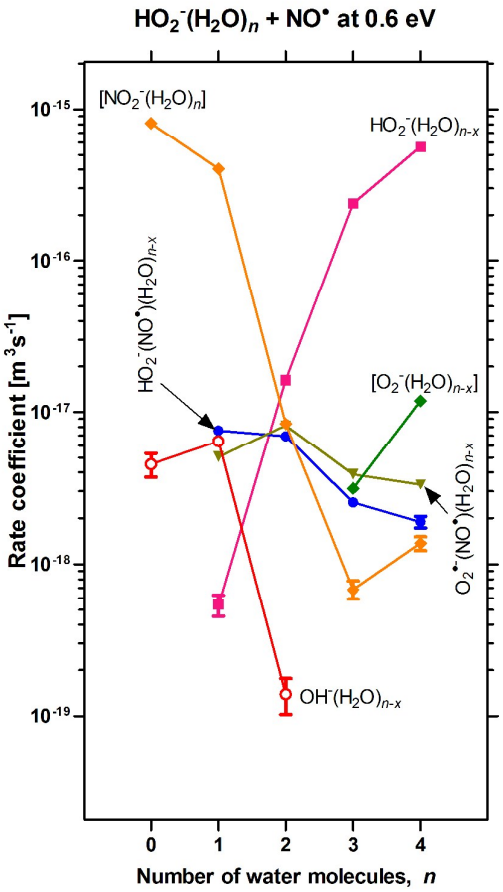

Figure 1. Rate coefficients for $HO_2^-(H_2O)_n$ + NO• leading to the various ionic products (summed over all values of *x*). The data are given for a centre-of-mass collision energy of 0.6 eV and different cluster sizes *n*. The absolute values of the rate coefficients are expected to be accurate within 25%. Error bars represent one SD due to count statistics. Products in square brackets can in addition be the result of contaminants, see the main text.

As seen in Figure 1, for the naked peroxide ion ($n = 0$) we observe two reaction products, NO_2^- and OH^-. They are identified as the products of the reactions,

$$HO_2^- + NO^\bullet \rightarrow NO_2^- + OH^\bullet, \text{ and} \qquad (3a)$$

$$\rightarrow OH^- + NO_2^\bullet; \qquad (3b)$$

with reaction 3a being about two orders of magnitude more frequent than reaction 3b. Using tabulated thermochemical data we estimate the two reactions to be exothermic by 136 and 93 kJ mol^{-1}, respectively.[40, 41] In addition, there is a possibility of NO_2^- being formed in a charge transfer

reaction to $NO_2^{\bullet}$ present as a contamination in the collision gas. This reaction,

$$HO_2^- + NO_2^{\bullet} \rightarrow NO_2^- + HO_2^{\bullet}, \quad (4)$$

is exothermic by 115 kJ mol^{-1}.[42] However, this reaction is estimated to be a largely insignificant contributor to the observed NO_2^- formation compared to the oxidation of $NO^{\bullet}$ (reaction 3a). This is based on the fact that the concentration of $NO^{\bullet}$ in the collision cell is vastly greater than that of $NO_2^{\bullet}$, the collision cross sections is similar between $NO^{\bullet}$ and $NO_2^{\bullet}$, and the energetics of reaction 3a is very favourable; these factors are discussed in more detail below. Bowie *et al.* reported the thermal rate coefficient for reaction 3a to be 5.0×10^{-16} m^3s^{-1} at 300 K.[34]

Both of the products, NO_2^- and OH^-, show decreasing reaction rates with increasing collision energy (Figure S1a). While the ion–neutral collision cross section is expected to shrink with increasing relative velocity, application of ion-molecule collision rate theory[43-46] using known molecular properties[47, 48] in agreement with relevant literature kinetic data[49] indicates that this effect should be negligible for the present case. This is discussed in more detail in the Supplementary Information together with alternative explanations.

Results for the quantum chemical computations of HO_2^- + $NO^{\bullet}$ are displayed in Figure 2. On this basis we propose a mechanism that accounts for the experimental observation of products, in particular the formation of NO_2^-. The first elementary step involves the formation of a reactant complex (**aINT1**), a species that requires some comments. The absolute value of the electric dipole moment of $NO^{\bullet}$ has been determined experimentally to have a small negative value of –0.15 D, corresponding to $N^{\delta-}O^{\delta+}$,[50, 51] in agreement also with accurate quantum chemical estimates.[52-55] For this reason it seems clear that the intermolecular bonding pattern seen for the reactant adduct **aINT1** is not governed by charge−charge interactions in the classical sense since the negative N-end of $NO^{\bullet}$ is attached to the negative end of the HO_2^- molecule. Closer inspection indicates that the interaction

instead is a combination of hydrogen bond, ion-induced dipole and charge-transfer. For the latter, the N atom acts as a weak electron acceptor as determined by its valence electronic configuration, $(\sigma_{2s})^2(\sigma_{2s}^*)^2(\pi_{2p_x})^2(\pi_{2p_y})^2(\sigma_{2p_z})^2(\pi_{2p_x}^*)^1$, in which the singly occupied molecular orbital (SOMO) has its dominating lobe at the nitrogen atom with the main component of the electron spin (computed spin density of 0.72 e, see Figure 2). In addition to this interaction, the reactant adduct (**aINT1**) is held together by a strong O–H···O hydrogen bond resulting in a side-on structure which lies 61.9 kJ mol^{-1} below the separate reactants. However, within the adduct, the negative charge remains mainly within HO_2^- (computed APT charge of –0.75 e) and the unpaired spin remains mainly within $NO^{\bullet}$; this in accordance with the closed-electronic shell of the ion and the radical character of the neutral and also the fact that the electron affinity of $HO_2^{\bullet}$ (*EA* = 1.08 eV)[40] is by far larger than that of $NO^{\bullet}$ (*EA* approximately 0.02–0.04 eV).[40]

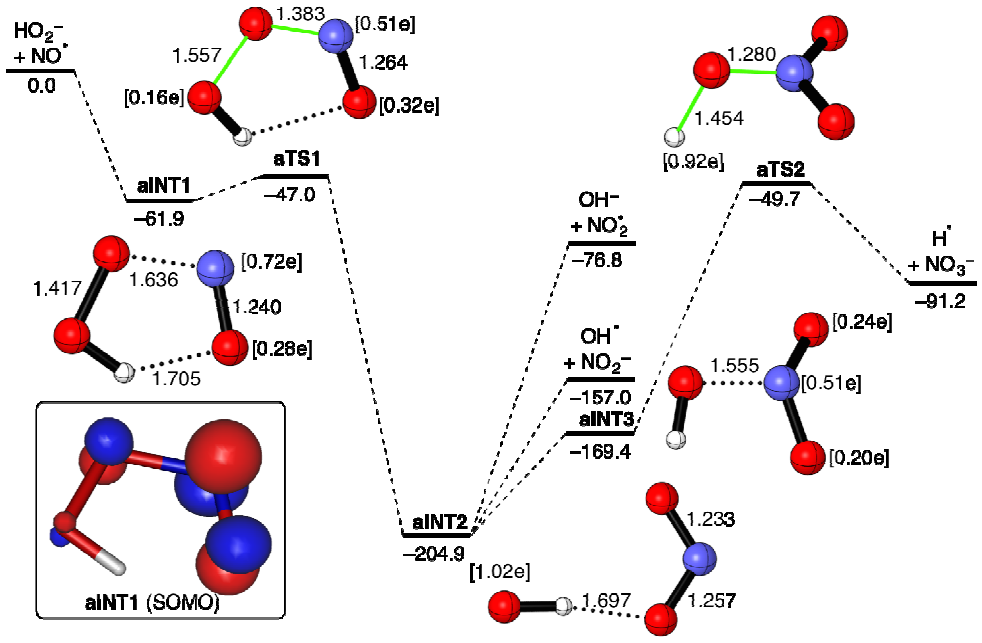

Figure 2. Computed potential energy profile (doublet electronic state) for the reaction between HO_2^- and $NO^{\bullet}$. Bond distances and relative free energies are given in angstroms and kJ mol^{-1}, respectively. Computed spin densities are given in square brackets. The inset represents the SOMO of intermediate **aINT1** (isosurface value of 0.05 au). All data have been computed at the uM06-2X/6-311+G(d,p) level.

The second elementary step is the highly exergonic formation of the $OH^{\cdots}ONO^-$ intermediate (**aINT2,** ΔG_R = –143.0 kJ mol^{-1}) from the reactant adduct (**aINT1**) via the transition state geometry **aTS1**. This saddle point is associated with easy formation ($\Delta G^{\neq}$ = 14.9 kJ mol^{-1}) of the new N···O bond and rupture of the O···O bond. This constitutes therefore the actual oxidation step, and it corresponds to the simultaneous transfer of an oxygen atom plus an electron from HO_2^- to $NO^{\bullet}$. From the bond lengths and in particular the spin densities, it can be seen that **aTS1** is positioned "early" along the generalized reaction coordinate, resulting from the large exergonic character of the reaction step (according to Hammond's postulate). The exergonicity, in turn, can largely be inferred from the very high electron affinity of $NO_2^{\bullet}$ (*EA* = 2.27 eV = 219 kJ mol^{-1}).[40] The intermediate **aINT2** is largely held together by a strong hydrogen bond. The two molecular entities $OH^{\bullet}$ and NO_2^- can be clearly distinguished within the complex, as evident by partial charges, bond parameters and spin densities (*i.e.* the unpaired electron is exclusively located at the oxygen atom of the OH moiety). Dissociation of the complex leads to NO_2^- + $OH^{\bullet}$ as the most favourable products from a thermochemical perspective at −157 kJ mol^{-1} (*cf.* −136 kJ mol^{-1} for the enthalpy change for reaction 3a, from tabulated thermochemical data). Alternatively, charge transfer to $OH^{\bullet}$ will lead to OH^- + $NO_2^{\bullet}$ at −76.8 kJ mol^{-1} (reaction 3b, exothermic by −93 kJ mol^{-1} from tabulated data). Qualitatively, this explains the experimentally observed product distribution in reasonable agreement with the aforementioned listed differences in energies of products and reactants.

We have also identified an alternative reaction pathway, via $[HO\cdots NO_2]^{\bullet-}$ (**aINT3**) and **aTS2**, which eventually would lead to NO_3^- formation upon H atom loss and further oxidation of the central nitrogen atom. Most likely, the internal rotation of the OH moiety, leading from **aINT2** to **aINT3**, has a negligible barrier and we were not able to locate the saddle point corresponding to a transition state geometry for this process. The formation of NO_3^- was not observed experimentally, and is

likely suppressed for purely entropical reasons; from the energetic reaction intermediate **aINT2**, the reaction is much more likely to quickly dissociate to form any of the product pairs NO_2^- + $OH^\bullet$ or OH^- + $NO_2^\bullet$ than to proceed through the tight transition state **aTS2** which constitutes an energy barrier only slightly lower than the OH^- + $NO_2^\bullet$ product asymptote.

For $HO_2^-(H_2O)$ we observe formation of NO_2^- and $NO_2^-(H_2O)$ as the two most abundant products in the experiments (grouped together in Figure 1),

$$HO_2^-(H_2O) + NO^\bullet \rightarrow NO_2^-(H_2O) + OH^\bullet \rightarrow NO_2^- + OH^\bullet + H_2O, \quad (5)$$

with NO_2^- being the clearly dominating product (Figure S1b in the Supplementary Information). In total, including $NO_2^-(H_2O)$, the nitrite formation rate is around 45% of the one observed for the unhydrated HO_2^- ion, clearly an effect of solvation. Obviously, the first step of reaction 5 is more exothermic than the complete reaction; the energies are, respectively, −111 kJ mol^{-1} and −46 kJ mol^{-1}, as calculated from thermochemical data.[40, 41, 56, 57] In general, products with excess energy due to an exothermic reaction will typically cool down by rapid evaporation of H_2O until they reach a point where the lifetime of the cluster at the current level of hydration and temperature is of the same order as the experimental time frame.[40, 41, 56, 57] As the binding energy of $NO_2^-(H_2O)$ is 65 kJ mol^{-1} we expect that this ion would fragment into NO_2^- + H_2O.[58] As discussed above, charge transfer from HO_2^- to contaminating $NO_2^\bullet$ is likely, but should not have significant impact on the detected NO_2^- abundance.

We have also observed a number of products of lower abundance. We find an exchange reaction in which $NO^\bullet$ is incorporated into the cluster upon loss of water:

$$HO_2^-(H_2O) + NO^\bullet \rightarrow HO_2^-(NO^\bullet) + H_2O. \quad (6)$$

As the molecular structure of the product ion in reaction 6 is not determined experimentally, we have opted to use the nominal notation $HO_2^-(NO^\bullet)$ for it here.

As with naked HO_2^-, we detect formation of hydroxide ions also for $HO_2^-(H_2O) + NO^\bullet$:

$$HO_2^-(H_2O) + NO^\bullet \rightarrow OH^-(H_2O) + NO_2^\bullet \rightarrow OH^- + NO_2^\bullet + H_2O. \quad (7)$$

In this case, only the monohydrated ionic product was detected (Figure S1b in the Supplementary Information). The first step is found to be exothermic by 115 kJ mol^{-1} using literature values for formation energies and electron affinities, while the second step is essentially thermoneutral at −2 kJ mol^{-1}.[40, 41, 56, 57]

Interestingly, an oxidation reaction giving rise to H atom loss,

$$HO_2^-(H_2O) + NO^\bullet \rightarrow O_2^{\bullet-}(NO^\bullet)(H_2O) + H^\bullet \rightarrow O_2^{\bullet-}(NO^\bullet) + H^\bullet + H_2O \quad (8)$$

was also identified, although only the final, unhydrated, ionic product was observed (Supplementary Information Figure S1b). Based on tabulated thermochemical data, the reaction enthalpy of the first step is −48 kJ mol^{-1}, while it is +11 for the full reaction, assuming the ionic product is nitrate, NO_3^-.[40, 41, 56, 57] The isomeric peroxynitrite, $ONOO^-$, already mentioned in the Introduction, has a formation enthalpy in solution that is 163 kJ mol^{-1} higher than that of nitrate and is an unlikely product in this case.[24]

For $HO_2^-(H_2O)$ we also observe some degree of dehydration caused by either collision induced dissociation (CID) or to spontaneous evaporation. We expect the former process to be the main contributor to the loss of H_2O, as this is typically the case for this kind of experiment,[20, 35] thus we consider the reaction to be

$$HO_2^-(H_2O) + NO^\bullet \rightarrow HO_2^- + NO^\bullet + H_2O, \quad (9)$$

which is endothermic by 90 kJ mol^{-1} but feasible due to the collision energy.[57]

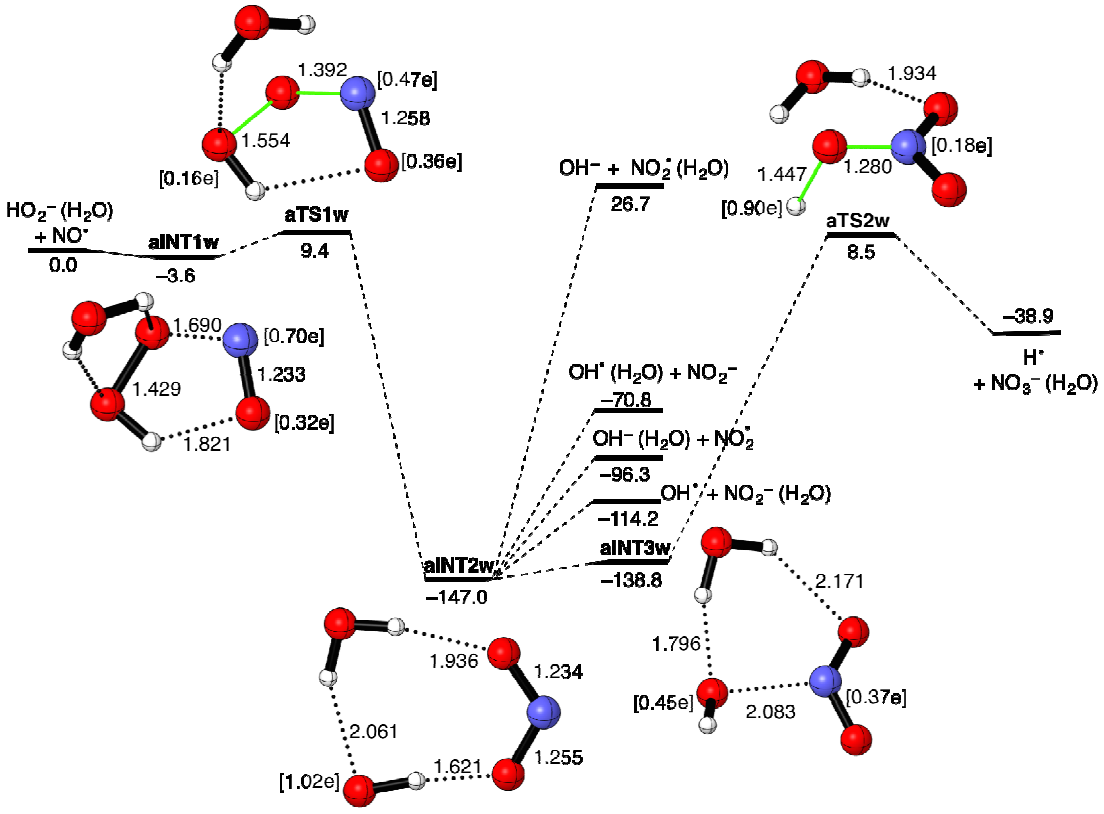

Figure 3. Computed potential energy profile (doublet electronic state) for the reaction between $HO_2^-(H_2O)$ and $NO^\bullet$. Bond distances and relative free energies are given in angstroms and kJ mol^{-1}, respectively. Computed spin densities are given in square brackets. All data have been computed at the uM06-2X/6-311+G(d,p) level.

The computational results for $HO_2^-(H_2O)$ are displayed in Figure 3. As seen, the reaction of the $HO_2^-(H_2O)$ cluster, whose structure resembles $HO^-(HOOH)$ as previously reported by Bierbaum and co-workers,[59] has all the essential qualitative features of the reaction of the naked HO_2^- ion. However, the energetics are significantly different. The $HO_2^-(H_2O) + NO^\bullet \rightarrow NO_2^-(H_2O) + OH^\bullet$ reaction is less exergonic than the corresponding dehydrated reaction ($\Delta\Delta G_R$ = 42.8 kJ mol^{-1}) due to the enthalpy of hydration of HO_2^- being higher than that of NO_2^-. All intermediate states are therefore higher in relative energy by approximately the same amount. This is clearly a solvation effect. Solvation of the reactant HO_2^- has a stabilizing effect by dispersing some of the negative charge onto the water molecule. This hampers electron transfer, which we have seen is a major

driving force for the oxidation reaction. We expect that the effect will be stronger the larger cluster is, explaining the experimentally observed drop in reactivity with size. This effect is well known in water cluster chemistry (see references mentioned by Ryding *et al.*, in particular Bohme *et al.*).[20, 60] This general drop in reactivity with increasing cluster size, and the thereby increasing degree of solvation of the core ion, is usually understood from a reaction model where the core ion needs to be activated by desolvation before reaction can occur.

We find in Figure 3 that the computed reaction free energy for the formation of $NO_2^-(H_2O)$ is in good agreement with the reaction enthalpy obtained from the literature: −111 kJ mol^{-1} for the first step of reaction 5 *vs.* −114.2 given in Figure 3. The second step of reaction 5 leads to formation of the naked nitrite ion with a total exothermicity of approximately −46 kJ mol^{-1} without considering clustering of H_2O and $OH^\bullet$; the corresponding computed value in Figure 3 includes the formation of $OH^\bullet(H_2O)$, which puts the exergonicity of the reaction at −70.8 kJ mol^{-1}.

The product of reaction 6, nominally $HO_2^-(NO^\bullet) + H_2O$, could correspond to the loss of H_2O from either of the reaction complexes **aINT1w** or **aINT2w**, thereby forming **aINT1** or **aINT2** (Figure 2), respectively. The computed free energies of the products relative to the reactants are +20.1 kJ mol^{-1} in the former case and −122.9 kJ mol^{-1} in the latter case. The fact that the formed product would have to be stable on the experimental time scale in order to survive until detection speaks against it being the **aINT2** complex $[OH\cdots NO_2]^{\bullet-}$ as this would likely fall apart into any of the product pairs indicated in Figure 2. In contrast, the **aINT1** complex $[HO_2\cdots NO]^{\bullet-}$, being slightly endergonic in its formation is a more likely candidate for the identity of the product.

From literature formation energies, electron affinities, and ion clustering energies we obtain reaction enthalpies for the first ($OH^-(H_2O)$) and second (OH^-) step of reaction 7 to be respectively −115 and

−2 kJ mol^{-1}. The corresponding free energies are −96.3 and +26.7 kJ mol^{-1} from the QCC. In terms of the pure numbers only, the QCC results are therefore more consistent with the experimental observation of that only $OH^-(H_2O)$ is formed.

Finally, we see that Figure 3 includes a reaction path to the formation of $NO_3^-(H_2O)$ occurring by loss of $H^\bullet$; the computed reaction enthalpy of −53.0 kJ mol^{-1} (ΔG_R = –38.9 in Figure 3) fits well with the value obtained from the literature of −48 kJ mol^{-1} for the first step of reaction 8. This product was—as already mentioned—observed experimentally in the form of the unhydrated nitrate ion, NO_3^-, *i.e.*, the complete reaction 8, which was nearly thermoneutral. The reaction is analogous to the reaction described in Figure 2 leading to the same product; however, while both the final product and the transition state are higher in energy for the reaction starting from $HO_2^-(H_2O)$ compared to the reaction starting from the naked HO_2^- ion, the fact is that such a product was observed experimentally in the former case but not in the latter case. The absence of NO_3^- formation from the reaction HO_2^- + $NO^\bullet$ was attributed to a transition state along the way to its formation and the reaction being more likely to proceed directly to the products NO_2^- + $HO^\bullet$ or HO^- + $NO_2^\bullet$. The presence of a water molecule and the extra degrees-of-freedom it introduces alleviates this effect by increasing the lifetime of the reaction intermediates (*i.e.* of **aINT2w** and **aINT3w**). Alternatively, evaporation of H_2O during the reaction could possibly alter the kinetics, *e.g.*, by producing a cooler reaction intermediate the reaction could proceed as **aINT2w** → **aINT2** → **aINT3** → NO_3^- + $H^\bullet$.

Many reactions of the process involving $HO_2^-(H_2O)$ were observed also for $HO_2^-(H_2O)_n$ clusters with n = 2–4. From Figure 1 it is clear that the reaction rate for the formation of $NO_2^{\bullet-}(H_2O)_{n-x}$ decreases with increasing cluster size, and this occurs in a quite dramatic fashion: from n = 1 there is an exponential decrease in the rate coefficient until n = 3, followed by a slight increase for n = 4. On the other hand, the CID loss of H_2O exhibits an equally dramatic increase in rate when the level of

hydration increases from $n = 1$ to $n = 4$. The formation of $OH^-(H_2O)_{n-x}$ clusters were observed only with very low intensity for $n = 2$, and not at all for $n > 2$. Both the $NO^\bullet$-incorporation reaction, forming $HO_2^-(NO^\bullet)(H_2O)_{n-x}$, and the $H^\bullet$ elimination reaction forming $O_2^-(NO^\bullet)(H_2O)_{n-x}$ or $NO_3^-(H_2O)_{n-x}$, were rather unaffected by the degree of hydration. Regarding the formation of $HO_2^-(NO^\bullet)(H_2O)_{n-x}$, we note that the typical number of H_2O lost is $x = 2$ at 0.6 eV collision energy and that loss of water from an aqueous cluster typically costs in the range 50–80 kJ mol^{-1}.[58]

In addition, for $n = 3, 4$ we observe a product corresponding to a hydrated superoxide cluster, *i.e.*, $O_2^{\bullet-}(H_2O)_{n-x}$. Formally, this reaction could correspond to

$$HO_2^-(H_2O)_n + NO^\bullet \rightarrow O_2^{\bullet-}(H_2O)_{n-x} + HNO + xH_2O; \quad (10)$$

however, this reaction is found to be endothermic already for low levels of hydration, the reaction enthalpies are +68 kJ mol^{-1} for $n = 0$ and +65 kJ mol^{-1} for $n = 1$ (based on tabulated thermochemical data).[40, 41] Alternatively, this reaction could be the result of a reaction with background $NO_2^\bullet$:

$$HO_2^-(H_2O)_n + NO_2^\bullet \rightarrow O_2^{\bullet-}(H_2O)_{n-x} + HONO + xH_2O, \quad (11)$$

a reaction which is found to be exothermic at −51 kJ mol^{-1} for $n = 0$ and −54 kJ mol^{-1} for $n = 1$ and $x = 0$.[40, 41] The number of water molecules lost in the reaction is mainly $x = 1$, with a minor contribution from $x = 2$ for $n = 4$. No ions were observed that would correspond to $x = 0$, which rules out the possibility that the observed intensity is simply $O_2^{\bullet-}(H_2O)_n$ ions leaking through the quadrupole mass filter (see the Experimental part of the Methods Section for details).

Computational results for $HO_2^{\bullet}$ radicals

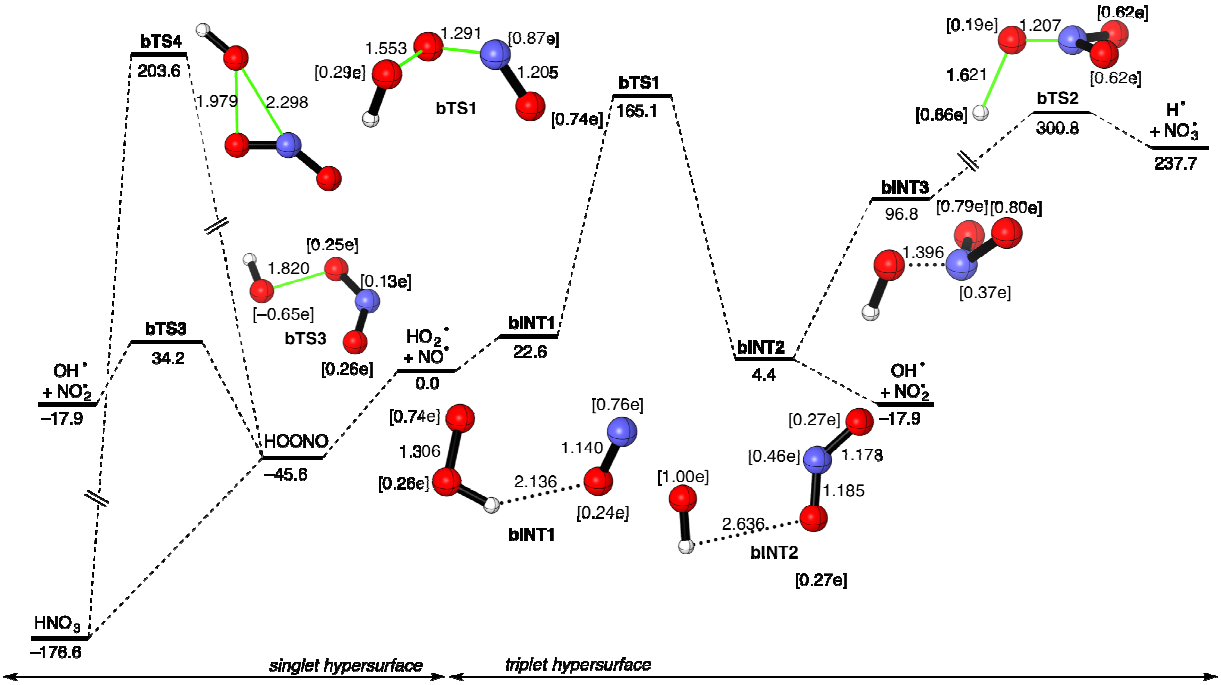

Figure 4. Computed potential energy profile (triplet electronic state) for the reaction between $HO_2^{\bullet}$ and $NO^{\bullet}$. Bond distances and relative free energies are given in angstroms and kJ mol^{-1}, respectively. Computed spin densities are given in square brackets. All data have been computed at the uM06-2X/6-311+G(d,p) level.

The reaction between neutral $HO_2^{\bullet}$ and $NO^{\bullet}$ was also investigated in detail because of its importance in atmospheric chemistry and other areas, as mentioned in the Introduction. With two free radical reactants, there are two available potential energy surfaces, one for the triplet electronic state and one for the singlet. We will first discuss the triplet state reaction. It is evident from Figure 4, that except for the energetics, the key elementary steps resembles those of HO_2^- + $NO^{\bullet}$, discussed above (Figure 2). In the first step, the formation of the initial adduct, $HO_2^{\bullet}\cdots NO^{\bullet}$ (**bINT1**), is slightly endergonic (ΔG_R = 22.6 kJ mol^{-1}) since spin pairing between the SOMO-electrons of $NO^{\bullet}$ and $HO_2^{\bullet}$ is avoided by the overall spin constraint. The transition state geometry of **bTS1** has much in common with **aTS1** of Figure 2, but since this reaction step is only slightly exergonic in the absence

of the effect of transferring the extra electron to the nascent NO_2 moiety ($\Delta G_R = -18.2$ kJ mol^{-1}), it is positioned later along the generalized reaction coordinate as evident from the bond lengths and spin densities (for instance, the N···O distance of 1.291 Å in **bTS1** is much shorter than in **aTS1**, 1.383 Å). In correspondence with this, the transition state geometry (**bTS1**) is rather high in energy at +165.1 kJ mol^{-1}, making the gas phase reaction rather sluggish in the triplet electronic state. The resulting weakly bonded product adduct $HO^{\bullet}\cdots NO_2^{\bullet}$ (**bINT2**) preserves the radical character of the two entities, and separation of **bINT2** leads to $HO^{\bullet} + NO_2^{\bullet}$ at –17.9 kJ mol^{-1} in an overall exergonic reaction, and fortuitously in quantitative agreement with the reaction enthalpy calculated from formation enthalpies.[41]

Also in this case we looked at possibilities for further oxidation, primarily to give $H^{\bullet} + NO_3^{\bullet}$. However, we find that this process is highly disadvantageous as it is endergonic by 237.7 kJ mol^{-1}, with a barrier at 300.8 kJ mol^{-1} for the passage of **bTS2** via the intermediate **bINT3**. The geometry of this transition state is rather similar to that computed for **aTS2** (Figure 2) but is clearly positioned later along the reaction coordinate (N···O distance of 1.207 Å in **bTS2** vs 1.280 Å for **aTS2**) due to energetically much higher products.

The alternative singlet electronic state of $HO_2^{\bullet} + NO^{\bullet}$ (the potential energy diagram for which is also depicted in Figure 4) allows for spin pairing and the formation of the covalently bonded HOONO, peroxynitrous acid at –45.6 kJ mol^{-1}. All our attempts to locate a transition state geometry associated with the formation of the new N···O bond met with no success, thereby suggesting this spin pairing may be considered as a barrierless process as confirmed by relaxed scans calculations (see Figure S5 in the Supplementary Information). Dissociation of the O–O bond via **bTS3** (activation barrier of 79.8 kJ mol^{-1}) would give $HO^{\bullet} + NO_2^{\bullet}$ with conservation of total electron spin. In summary, reaction in the singlet state is by far the kinetically preferred gas phase route to $NO_2^{\bullet}$. Our QCC also show

that peroxynitrous acid may rearrange to the thermodynamically more stable nitric acid via the transition state **bTS4**. However, the considerable barrier of 242.9 kJ mol^{-1} (from HOONO) for this highly interesting isomerization reaction is prohibitively large for a thermal gas phase reaction, and is therefore not expected to occur. These aspects have been investigated previously, including by quantum chemical computations, reaching the same conclusion as here.[61-65]

Experimental and computational results for $O_2^{\bullet-}$ clusters

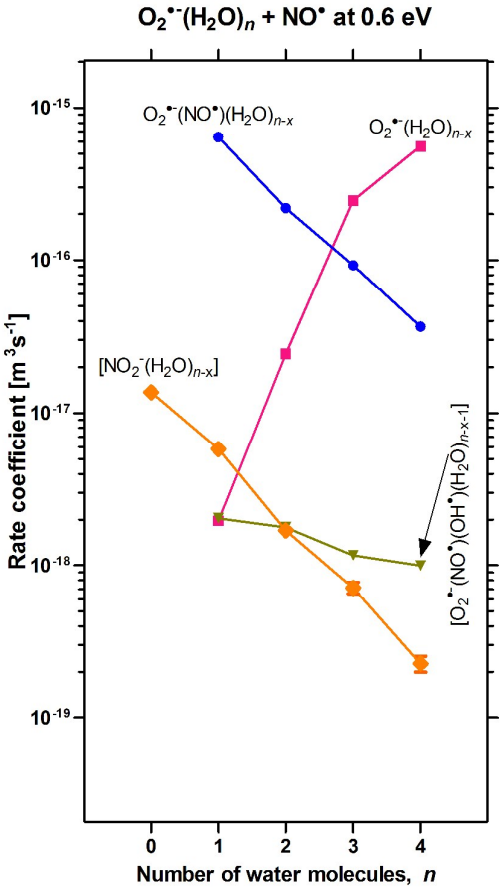

Figure 5. Rate coefficients for $O_2^{\bullet-}(H_2O)_n$ + $NO^{\bullet}$ leading to the indicated ionic products (summed over all values of *x*). The data are given for a centre-of-mass collision energy of 0.6 eV and different cluster sizes *n*. The absolute values of the rate coefficients are expected to be accurate within 25%. Error bars represent one SD due to count statistics. Products in square brackets can also be the result of reaction with contaminants, see the main text.

The experimental findings for the reaction of $NO^{\bullet}$ with superoxide (hydrated by 0–4 water molecules) at 0.6 eV centre-of-mass collision energy, are summarized in Figure 5. The Supplementary Information (Figure S2) contains data also for some different collision energies and also shows how many water molecules are lost for the different reaction pathways.

The dominant reaction for n = 1, 2 is ligand substitution, in which H_2O is replaced by $NO^{\bullet}$. For larger clusters water evaporation due to collisionally induced decomposition is dominating. These reactions will be discussed below. For naked $O_2^{\bullet-}$ we have only detected one product of significant abundancy, and that is formation of NO_2^-, which a priori could be due to the reaction:

$$O_2^{\bullet-} + NO^{\bullet} \rightarrow NO_2^- + {}^3O. \qquad (12)$$

This reaction is only slightly endothermic at +16 kJ mol^{-1},[40, 41] and is in principle within reach given the collision energy of 0.6 eV = 58 kJ mol^{-1}; however, as discussed below, the reaction is associated with a substantial reaction barrier which makes us conclude that it is not feasible. Instead, we propose that the observed NO_2^- formation is due to a charge transfer reaction to the $NO_2^{\bullet}$ gas present in the collision cell as a contaminant, *i.e.*,

$$O_2^{\bullet-} + NO_2^{\bullet} \rightarrow NO_2^- + O_2 \qquad (13)$$

which is exothermic by 176 kJ mol^{-1}.[40] The recorded abundance of NO_2^- is in good accord with the fact (see Supplementary Information) that $NO_2^{\bullet}$ is present at the 1% level relative to $NO^{\bullet}$ and also with the high cross section for exothermic electron transfer reactions.

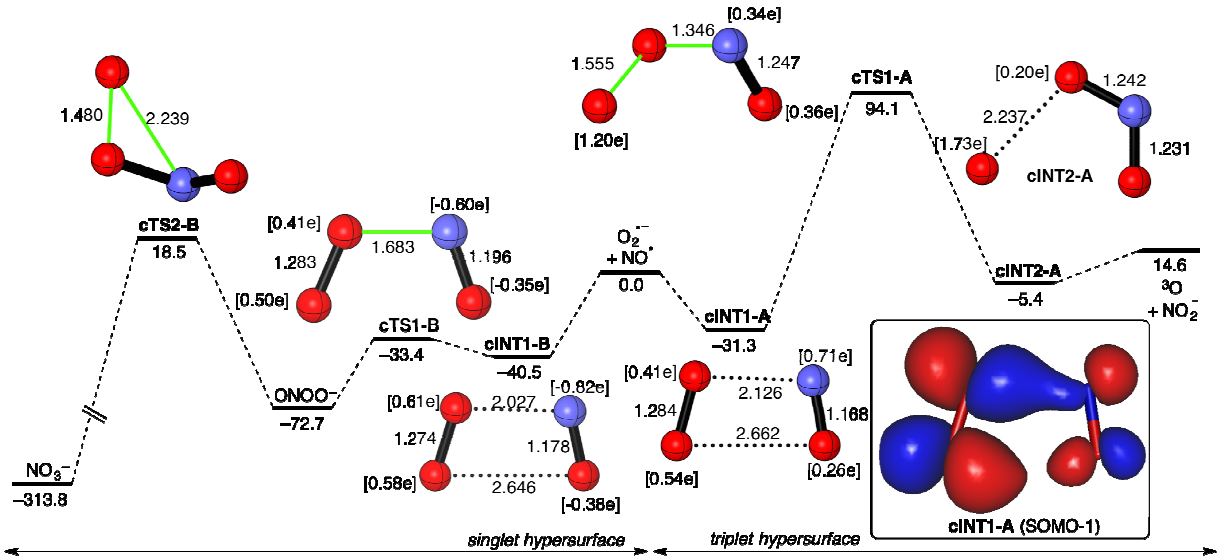

Figure 6. Computed potential energy profile (singlet and triplet electronic state) for the reaction between $O_2^{\bullet-}$ and $NO^{\bullet}$. Bond distances and relative free energies are given in angstroms and kJ mol^{-1}, respectively. The inset represents the SOMO of intermediate **cINT1-A** (isosurface value of 0.05 au). Computed spin densities are given in square brackets. All data have been computed at the uM06-2X/6-311+G(d,p) level.

The computational results for the possible oxidation of $NO^{\bullet}$ in reactions with $O_2^{\bullet-}$ is presented in Figure 6. This system is isoelectronic to $HO_2^{\bullet}$ + $NO^{\bullet}$, so both the triplet and singlet hypersurfaces have to be considered.

On the triplet potential energy surface we find a route to reaction 12, formation of NO_2^-, which proceeds through two intermediates with a reaction barrier. The reactant adduct **cINT1-A** is bonded by considerable ion-induced dipole forces but with little charge and spin transfer, and we note that the O···N contact is shorter than the O···O contact, indicating some orbital interaction at this stage. Indeed, inspection of the SOMO-1 (see inset in Figure 6) clearly indicates that the orbital interaction involving the in-plane π-molecular orbitals is stronger between the O···N atoms. The following **cINT1-A** → **cINT2-A** step via the transition state geometry **cTS1-A** is endergonic (ΔG_R = +25.9 kJ mol^{-1}) and proceeds with a relatively high activation barrier of 125.4 kJ mol^{-1} (94.1 kJ mol^{-1} relative

to the reactants). This is sharply different to the analogous process involving HO_2^- (Figure 2), which is highly exergonic and proceeds with a rather low barrier. This finding suggests that the occurrence of the intramolecular hydrogen bond in the process involving HO_2^- controls the simultaneous formation of the new N···O bond and rupture of the O···O bond by bringing the reactants closer together. The product complex **cINT2-A** at −5.4 kJ mol^{-1} is essentially a weakly bonded complex between ^3O and NO_2^- with some residual spin exchange to NO_2^-. This complex, if formed, may then dissociate to give separated $^3O + NO_2^-$ at +14.6 kJ mol^{-1} in good agreement with the +16 kJ mol^{-1} for the enthalpy change obtained from tabulated thermochemical data. The singlet oxygen atom was not considered as a feasible neutral product in this reaction since it is too high in energy. It should also be mentioned that the negative charge is key to reactivity also in this case. The corresponding reaction $^3O_2 + NO^\bullet \rightarrow NO_2^\bullet + {}^3O$ is calculated to be both prohibitively endergonic and having a very high energy barrier (see QCC results in Supplementary Information).

Of particular note for the reaction on the triplet hypersurface is the reaction barrier **cTS1-A** at +94.1 kJ mol^{-1} relative to the reactants. This is similar in magnitude compared to the collision energy of 0.6 eV and this should prove prohibitive to the reaction occurring under the current experimental conditions. A look at the experimentally detected formation of NO_2^- at different collision energies (Figure S2) shows that this reaction does not become more frequent as collision energy increases, in fact it seems to have a slight decrease. However, as discussed in the Supplementary Information, there are several other factors that influence the trends in observed product abundance with changing collision energies.

We will now consider the energy profile for the putative reaction:

$$O_2^{\bullet-} + NO^\bullet \rightarrow ONOO^- \rightarrow NO_3^-. \qquad (14)$$

This reaction was not observed experimentally, but is energetically favourable by being exothermic

by 356 kJ mol^{-1} (from tabulated thermochemical data). [40, 41] Moreover, the computations indicate that there is a downhill path on the singlet hypersurface leading to the nitrate anion, illustrated on the left hand side of Figure 6; the reaction enthalpy obtained by the QCC, –357.9 kJ mol^{-1} (ΔG_R = –313.8 kJ mol^{-1}), is in good agreement with the value given above. In close analogy with the reaction of $HO_2^\bullet$ and $NO^\bullet$ (Figure 4) we find that $O_2^{\bullet-}$ and $NO^\bullet$ may form a covalent adduct $ONOO^-$, peroxynitrite, at –72.7 kJ mol^{-1}, through transition state geometry **cTS1-B** (analogous to **cTS1A** on the triplet hypersurface in Figure 6). Peroxynitrite can then be transformed into NO_3^- via the transition state geometry **cTS2-B** with an activation barrier of 91.2 kJ mol^{-1} (18.5 kJ mol^{-1} relative the reactants) in a highly exergonic process (−241.1 kJ mol^{-1}). The corresponding isomerisation of peroxynitrite to nitrate in solution is exothermic by 163 kJ mol^{-1}.[24] However, the formation of stable NO_3^- or $ONOO^-$ requires stabilizing collisions of the short-lived adducts, which is only possible at higher pressures than accessible in our experiments.

For $O_2^{\bullet-}(H_2O)$ + $NO^\bullet$, we observe four types of product ions in the experiments (Figure 5). The most abundant is due to $NO^\bullet$ incorporation upon water loss

$$O_2^{\bullet-}(H_2O) + NO^\bullet \rightarrow O_2^{\bullet-}(NO^\bullet)(H_2O) \rightarrow O_2^{\bullet-}(NO^\bullet) + H_2O. \qquad (15)$$

As with the incorporation reaction for $HO_2^{\bullet-}$, the chemical nature of the product ion is unknown and we opt to use a nominal notation for it here; however, likely product ions are peroxynitrite or nitrate in light of this reaction being the hydrated analogue of reaction 14. Assuming NO_3^- as the product, reaction 15 is exothermic by 322 kJ mol^{-1} for the first step and by 262 kJ mol^{-1} for the total reaction (based on tabulated thermochemical data).[40, 41, 56] From this we also estimate that the reaction in question would still be exothermic should the formed product be peroxynitrite.[24]

The second most abundant product observed (Figure 5) for $O_2^{\bullet-}(H_2O)$ is the formation of NO_2^-, which could be due to

$$O_2^{\bullet-}(H_2O) + NO^{\bullet} \rightarrow NO_2^-(H_2O) + {}^3O \quad (16a)$$

$$\rightarrow NO_2^- + {}^3O + H_2O. \quad (16b)$$

$$\rightarrow NO_2^- + H_2O_2. \quad (16c)$$

Again, this product is most likely due to reaction with the contaminant $NO_2^{\bullet}$:

$$O_2^{\bullet-}(H_2O) + NO_2^{\bullet} \rightarrow NO_2^-(H_2O) + O_2 \rightarrow NO_2^- + O_2 + H_2O. \quad (17)$$

Reaction enthalpies based on thermochemical data are as follows: reaction 16a, +44 kJ mol^{-1}; reaction 16b, +109 kJ mol^{-1}; and reaction 16c, −34 kJ mol^{-1}. [40, 41, 56] However, as shown by the QCC results in Figure 7, there is a substantial reaction barrier associated with these reactions. For reaction 17, the reaction enthalpies as calculated from thermochemical data are −148 kJ mol^{-1} for the first step and –83 kJ mol^{-1} for the second step.[40, 41, 56] Experimentally, we detect approximately equal amounts (45:55) of NO_2^- and $NO_2^-(H_2O)$ (Figure S2b in the Supplementary Information).

We observe some degree of collisionally induced dissociation for $O_2^{\bullet-}(H_2O)$:

$$O_2^{\bullet-}(H_2O) + NO^{\bullet} \rightarrow O_2^{\bullet-} + NO^{\bullet} + H_2O \quad (18)$$

A process that is endothermic by 90 kJ mol^{-1}.[56]

In addition, we detect a product ion that is consistent with H-atom loss,

$$O_2^{\bullet-}(H_2O) + NO^{\bullet} \rightarrow O_2^{\bullet-}(NO^{\bullet})(OH^{\bullet}) + H^{\bullet}. \quad (19)$$

However, thermochemical analysis precludes this reaction as no feasible product could be identified (also when considering a possible reaction with $NO_2^{\bullet}$). Taking the low signal level into account, we cannot rule out that experimental artefacts are responsible for the observed abundance.

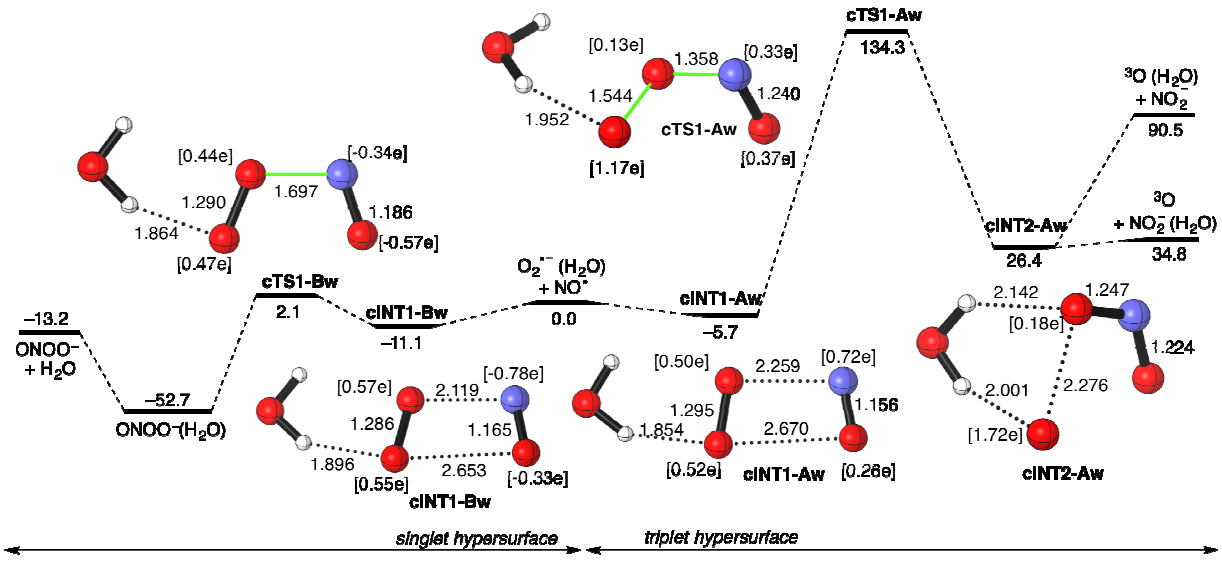

Figure 7. Computed potential energy profile (singlet and triplet electronic state) for the reaction between $O_2^{\bullet-}(H_2O)$ and $NO^\bullet$. Bond distances and relative free energies are given in angstroms and kJ mol^{-1}, respectively. Computed spin densities are given in square brackets. All data have been computed at the uM06-2X/6-311+G(d,p) level.

The conclusions on the influence of hydration that can be drawn from the computed reaction profile involving $O_2^{\bullet-}(H_2O)$ and $NO^\bullet$ in Figure 7 are similar to those already discussed for the HO_2^- case. Again, dispersion of the negative charge by the water molecule leads to a slight increase in the reaction barrier involving **cTS1-Aw** (140.0 kJ mol^{-1} relative to the preceding reaction intermediate *vs.* 125.4 kJ mol^{-1} for the analogous, unhydrated **cTS1-A** in Figure 6). We also note that the central elementary oxidation step (**cINT1-Aw** → **cINT2-Aw**) is endergonic by 32.1 kJ mol^{-1} for the hydrated intermediate, while it is less endergonic at 25.9 kJ mol^{-1} for the bare species (**cINT1-A** → **cINT2-A** in Figure 6), in agreement with the slightly higher barrier in the hydrated case.

According to our QCC, the reaction on the singlet hypersurface leading to the formation of hydrated peroxynitrite (reaction 15) is exergonic at −52.7 kJ mol^{-1}. In contrast to the case of the naked superoxide ion, this reaction involves a means by which the formed product can rid itself of excess energy and stabilize: evaporation of H_2O. This is consistent with the computed energy for the

product pair $ONOO^-$ + H_2O at –13.2 kJ mol^{-1} in Figure 7 and the experimental observation that the observed product was unhydrated. Isomerisation to NO_3^- (not included in Figure 7) would still produce a rather hot product.

On the triplet hypersurface, the reaction leading to $NO_2^-(H_2O)$ is found to be endergonic at +34.8 kJ mol^{-1} relative to the reactants. The corresponding reaction enthalpy determined from literature thermochemical data was +44 kJ mol^{-1}. The substantial reaction barrier of 134.3 kJ mol^{-1} relative to the reactants should make this reaction impossible under current experimental conditions. Consequently, we conclude that detected formation of NO_2^- is due to the charge transfer reaction involving background $NO_2^{\bullet}$ (reaction 17). On this premise we can directly estimate the degree of $NO_2^{\bullet}$ contamination in the $NO^{\bullet}$ collision gas from the experimental results in Figure 5. Assuming similar reaction cross-section for the incorporation reaction with $NO^{\bullet}$ (reaction 15) and charge transfer reaction with $NO_2^{\bullet}$ (reaction 17) the relationship $NO^{\bullet}$: $NO_2^{\bullet}$ would be 0.9911:0.0088. This is discussed further in the Supplementary Information.

We shall make a few observations regarding the experimental results of $O_2^{\bullet-}(H_2O)_n$ + $NO^{\bullet}$ as the hydration of the reactant ion increases above n = 1. As seen in Figure 5, as the hydration of the superoxide ion increases, the incorporation reaction (reaction 15) is found to decrease. This is a consequence of the solvation shell around the superoxide ion preventing $NO^{\bullet}$ from contacting $O_2^{\bullet-}$ and reacting, an effect that is often observed for water clusters.[20] Addition of $NO^{\bullet}$ to the cluster-ion without forming covalent bonds means that $NO^{\bullet}$ is susceptible to evaporation, thereby reforming the reactant cluster, especially if the binding energy of $NO^{\bullet}$ to the cluster is lower than that of the water molecules. A closer look at the number of water molecules lost in reaction 15 shows that when the superoxide reactant is hydrated by 3–4 water molecules, the typical number is $2H_2O$ lost (Figure S2 in the Supplementary Information). The number of water molecules lost depends upon the

condensation energy of $NO^{\bullet}$ as it enters the cluster, the collision energy, and also the reaction energy. In this case, the reaction energy is dependent upon which of the possible products—peroxynitrite or nitrate—that is being formed, *i.e.*, if the reaction on the singlet hypersurface stops at $ONOO^-$ or if it proceeds to NO_3^-. As mentioned above, in solution the formation energy of $ONOO^-$ is found to be 163 kJ mol^{-1} higher than that of NO_3^-.[24] We can also see from our QCC in Figure 6 that the corresponding free energy change in the gas phase should be approximately 241 kJ mol^{-1}. The fact that these larger clusters do not lose more water molecules—the evaporation energies of which usually lies between 50–80 kJ mol^{-1}—in this reaction indicates that the formed ionic product is the less exothermic one, *i.e.*, peroxynitrite.[58]

The formation of NO_2^- from $O_2^{\bullet-}(H_2O)_n$ is in the superoxide case observed to decrease substantially, in an almost exponential fashion, when n increases above 1. The hydration of the formed NO_2^- product can be summarized as follows: for n = 1, 72–80% NO_2^- and 20–28% $NO_2^-(H_2O)$; for n = 2, 61–67% NO_2^-, 33–39% $NO_2^-(H_2O)$ and 0% $NO_2^-(H_2O)_2$; for n = 3, 11–43% NO_2^-, 39–65% $NO_2^-(H_2O)$ and 18–23% $NO_2^-(H_2O)_2$; for n = 4, 0% NO_2^-, 65–78% $NO_2^-(H_2O)$ and 22–35% $NO_2^-(H_2O)_2$. If the formation of NO_2^- is due to a charge transfer reaction to contaminating $NO_2^{\bullet}$, it is likely—given the degree of hydration observed—that this reaction involves an intermediate of sufficient lifetime to transfer also water molecules to the nascent anion; alternatively, we can envision a stepwise mechanism in which $NO_2^{\bullet}$ enters the cluster, the charge transfer occur, and O_2 leaves the cluster. Regardless, it is clear that the charge transfer reaction is hampered by the presence of water molecules on the superoxide ion.

The collisionally induced dissociation reaction (reaction 18) increases with the number of water molecules in a fashion similar to that which was observed for the $HO_2^-(H_2O)_n$ clusters.

Methods

Experimental part

The experiments were performed using a quadrupole–time-of-flight mass spectrometer (QTOF); the instrument has also been described in previous publications.[35-39] The mass spectrometer has been modified with a stainless steel inlet system fitted with an ultra-high vacuum leak-valve; this allows for injection of volatile and semi-volatile compounds into the collision-cell.

Ions were produced in the electrospray ionization (ESI) unit fitted to the instrument. This unit was operated at room temperature and atmospheric pressure. Of the ESI gas flows available on the instrument—for nebuliser gas, desolvation gas and cone gas—only the nebuliser gas was used (adjusted until satisfactory conditions for ion production were obtained). Water (HiPerSolv Chromanorm for HPLC, VWR BDH Prolabo) was fed through the electrospray capillary at a rate of 25 μL min^{-1}. A weak corona discharge was obtained at the ESI needle tip by applying a voltage of 3.0–3.5 kV and positioning it close the inlet skimmer; this results in the formation of several types of anionic water-clusters, *e.g.*, $OH^-(H_2O)_n$, $O_3^-(H_2O)_n$, $HO_2^-(H_2O)_n$ and $O_2^{\bullet-}(H_2O)_n$. The ions were transferred into the high vacuum part of the instrument, where a quadrupole mass filter allowed for transmission of a single cluster size based on the cluster's mass-to-charge ratio (m/z).

Setting the width of the quadrupole selection window is a compromise between high sensitivity and high throughput of ions. Of particular concern is the selection of $HO_2^-(H_2O)_n$ ions. These are significantly less abundant than the $O_2^{\bullet-}(H_2O)_n$ ions which prohibits the quadrupole selection window to be set too narrow; on the other hand, setting the mass window too wide will result in the latter ions leaking though and influencing the measurements of the former. The solution employed was to use a rather wide mass selection window (approximately unit resolution) and positioning it somewhat off-centre, *e.g.*, for the $HO_2^-(H_2O)_n$ ions the quadrupole selection mass was given as the

actual value +0.2 Da. Separate background measurements performed without $NO^{\bullet}$ present in the collision cell was used to identify peaks that leak through the quadrupole mass window. For $O_2^{\bullet-}(H_2O)_n$, no peaks were observed at −1 Da relative to the parent ion and only for $O_2^{\bullet-}(H_2O)_4$ was a peak observed at +1 Da (likely $HO_2^-(H_2O)_4$). For $HO_2^-(H_2O)_n$, peaks were observed at +1 Da for n = 3, 4 and at −1 Da for n = 2 (likely $O_2^{\bullet-}(H_2O)_2$). None of these peaks were included in the reported product abundance. Furthermore, the abundance of these trace ions were so low relative to the abundance of the parent ion that their contribution to the detected product ion spectra would be insignificant should they react with $NO^{\bullet}$.

After leaving the quadrupole, the ions entered the collision cell (length 16 cm, with hexapole ion guide) at a well-defined lab-frame kinetic energy. $NO^{\bullet}$ (AGA, 2.5, 99.5%) was introduced into the collision cell using the above mentioned stainless steel inlet system; a cold trap (−114 °C, liquid nitrogen/ethanol) was set up between the gas flask and the ultra-high vacuum leak-valve (as close as possible to the latter) in order to remove contaminants, in particular $NO_2^{\bullet}$. However, some background $NO_2^{\bullet}$ (≤ 1%) was observed in the experiments (see also the Supplementary Information).

The $NO^{\bullet}$ pressure was adjusted using the ultra-high vacuum leak-valve in order to limit double collisions while maintaining a sufficiently high collision frequency to avoid problems with signal-to-noise ratios and count statistics; unfortunately, it is not possible to have an optimal $NO^{\bullet}$ pressure in this sense for all ions measured as the experiment aimed to cover ion–gas reactions occurring at different levels of ion hydration and collision energy. The pressure used was approximately 2.3–2.4×10^{-4} mbar, at which the maximum attenuation in the reactant ion current was estimated to 25% and the minimum to < 1%. In order to detect variations in the collision gas pressure during the course of the experiment, reference measurements were conducted at regular intervals (every eight measurements) using the $O_2^{\bullet-}(H_2O)_2$ ion at 0.6 eV (COM) collision energy.

Detection of products and reactants was done by the time-of-flight (TOF) unit fitted with a chevron type micro-channel-plate (MCP) detector. The MCP detector voltages were calibrated before the experiment until the isotopic pattern of $Na^+(NaCl)_n$ clusters were faithfully reproduced; this ensured that no bias towards larger or smaller mass spectrum peaks existed. The sodium chloride clusters were produced from a 30 mM NaCl(aq) solution (NaCl: 99.5%, Prolabo) and using a higher temperature (100 °C) on the ESI source.

The present experimental setup does unfortunately not allow for an accurate reading of the $NO^{\bullet}$ pressure, partly because some nitrogen gas from the ESI unit will leak into the collision cell. We expect the $NO^{\bullet}$ pressure to be within 20% of the pressure reading on the collision cell. The reference measurements show that while there is some uncertainty regarding the absolute $NO^{\bullet}$ pressure, the pressure is fairly stable over the course of a measurement series, changing by no more than 3% and with a slow drift. The latter variation has been compensated for in the experimental data.

Computational details

Quantum chemical computations were carried out using the GAUSSIAN 09 suite of programs.[66] All structures (reactants, transition structures, and products) were characterized by complete geometry optimization using the metahybrid functional M06-2X in conjunction with the triple-ζ quality 6-311+G(d,p) basis set.[67, 68] Reactants and products were characterized by frequency calculations,[69] and have positive definite Hessian matrices. Transition structures (TS's) show only one negative eigenvalue in their diagonalized force constant matrices, and their associated eigenvectors were confirmed to correspond to the motion along the reaction coordinate under consideration using the Intrinsic Reaction Coordinate (IRC) method.[70]

Final discussion and conclusions

The naked HO_2^- ion was observed to effectively oxidise $NO^\bullet$, thereby forming NO_2^-; in addition, formation of OH^- was observed to occur at a rate two orders of magnitude lower. The QCC indicate a pathway from $HO_2^- + NO^\bullet$ to NO_3^- by means of $H^\bullet$ loss but this was not observed experimentally. It appears that in the competition between the different reaction pathways, all starting from the same energetic $\{[OH\cdots NO_2]^{\bullet-}\}^*$ reaction intermediate, the path to NO_3^- is disfavoured because it involves one additional tight transition state, whereas the path to the other products is a simple dissociation of the $[OH\cdots NO_2]^{\bullet-}$ complex and allocation of the charge-carrying electron. Interestingly, the presence of water molecules enables the formation of NO_3^- from $HO_2^-(H_2O)_n$ clusters due to kinetic factors. As hydration of HO_2^- increases, the efficiency of $NO^\bullet$ oxidation was observed to decrease dramatically, in agreement with general trends known from water cluster chemistry.

In contrast to naked HO_2^-, naked $O_2^{\bullet-}$ does not give rise to products in direct reaction with $NO^\bullet$ at the low pressures of our study. However, $O_2^{\bullet-}(H_2O)_n$ clusters were observed to react with $NO^\bullet$ in a reaction in which the nitrogen monoxide molecule enter the cluster and water molecules leave it. This reaction was comparable in efficiency to the $NO^\bullet$-oxidation by HO_2^-, although not as sensitive to the degree of ion hydration. The QCC indicate that the incorporation reaction involves the formation of a peroxynitrite core ion, $O_2^{\bullet-} + NO^\bullet \rightarrow ONOO^-$, a reaction known from biochemistry to occur *in vivo*.[22] While peroxynitrite in principle can isomerize to nitrate, the experimental findings suggest that this is not the case for the isolated gas phase reactions studied here. However, this interesting question cannot be answered fully without spectroscopic characterization of the product ions. It is of note that the formation of $ONOO^-$ from $O_2^{\bullet-}(H_2O)_n + NO^\bullet$, similarly to the formation of NO_3^- from $HO_2^-(H_2O)_n + NO^\bullet$, was not observed experimentally for the naked ion, *i.e.*, $n = 0$. The explanation is also similar: the formation of peroxynitrite from $O_2^{\bullet-} + NO^\bullet$ is highly exothermic and the product will not survive under the current experimental conditions unless it has the opportunity

to be stabilized by evaporation of H_2O.

A crucial difference between the reactions of $O_2^{\bullet-}(H_2O)_n$ + $NO^{\bullet}$ and $HO_2^{-}(H_2O)_n$ + $NO^{\bullet}$ is that the former can (at least potentially) react on both the singlet and triplet hypersurfaces, while the latter reacts on the doublet hypersurface alone. The reaction of $O_2^{\bullet-}(H_2O)_n$ leading to $ONOO^-$ occurs on the singlet hypersurface. The reactions of the $HO_2^{\bullet}$ radical with $NO^{\bullet}$ is isoelectric to $O_2^{\bullet-}$ + $NO^{\bullet}$ and can therefore be viewed as having more in common with $O_2^{\bullet-}$ + $NO^{\bullet}$ than with HO_2^- + $NO^{\bullet}$.

Besides the relevance to atmospheric chemistry, insights obtained from this study could inspire the investigation of using anionic reactive oxygen species to oxidize NO_x in flue gases.

Acknowledgments

This work was supported by the Norwegian Research Council by the Grants No. 205512/F20, Nano-solvation in Hydrogen-Bonded Clusters; No. 179568/V30, to the Centre of Theoretical and Computational Chemistry through their Centre of Excellence program; and the Norwegian Supercomputing Program (NOTUR) through a grant of computer time (Grant No. NN4654K). The Spanish MINECO-FEDER (grants CTQ2013-44303-P and CTQ2014-51912-REDC) and NILS Project (002-ABEL-CM-2013) are gratefully acknowledged.

Supplementary Information Available

The Supplementary Information contains figures showing all detected reaction channels for $HO_2^{-}(H_2O)_n$ + $NO^{\bullet}$ and $O_2^{\bullet-}(H_2O)_n$ + $NO^{\bullet}$ at some different collision energies. In addition, the Supplementary Information includes a discussion on the degree of NO_2-contamination; computational results for $HO_2^{\bullet}(H_2O)$ and O_2; a discussion on calculated collisional cross-sections and rates of reactions for $NO^{\bullet}$ and $NO_2^{\bullet}$; and Quantum Chemical Computation data (geometries and

energies).

References

1. U. Schumann and H. Huntrieser, *Atmos. Chem. Phys.*, 2007, **7**, 3823-3907.
2. G. J. Leigh, *The World's Greatest Fix: A history of nitrogen and agriculture*, Oxford University Press, New York, 2004.
3. K. Annamalai and I. K. Puri, *Combustion Science and Engineering*, CRC Press, Boca Raton, 2007.
4. *JP Pat.*, JPS4815766B1, 1973.
5. *JP Pat.*, JPS8083-069, 1973.
6. *US Pat.*, US3991167 A, 1976.
7. *US Pat.*, US20050214187A1, 2005.
8. M. Koebel, M. Elsener and G. Madia, *Ind. Eng. Chem. Res.*, 2001, **40**, 52-59.
9. B. J. Tyler, *Nature*, 1962, **195**, 279-280.
10. D. Gray, E. Lissi and J. Heicklen, *J. Phys. Chem.*, 1972, **76**, 1919-1924.
11. R. Atkinson, D. L. Baulch, R. A. Cox, J. N. Crowley, R. F. Hampson, R. G. Hynes, M. E. Jenkin, M. J. Rossi and J. Troe, *Atmos. Chem. Phys.*, 2004, **4**, 1461-1738.
12. P. J. Crutzen, *Annu. Rev. Earth Pl. Sc.*, 1979, **7**, 443-472.
13. R. Reiter, *Tellus*, 1970, **22**, 122-136.
14. L. J. Ignarro, J. M. Fukuto, J. M. Griscavage, N. E. Rogers and R. E. Byrns, *P. Natl. Acad. Sci. USA*, 1993, **90**, 8103-8107.
15. K. Sekimoto and M. Takayama, *J. Electrostat.*, 2012, **70**, 363-373.
16. J. D. Skalny, T. Mikoviny, S. Matejcik and N. J. Mason, *Int. J. Mass Spectrom.*, 2004, **233**, 317-324.
17. K. Nagato, Y. Matsui, T. Miyata and T. Yamauchi, *Int. J. Mass Spectrom.*, 2006, **248**, 142-147.
18. K. Drenck, P. Hvelplund, S. B. Nielsen, S. Panja and K. Stochkel, *Int. J. Mass Spectrom.*, 2008, **273**, 126-131.
19. P. Hvelplund, U. Kadhane, S. B. Nielsen, S. Panja and K. Stochkel, *Int. J. Mass Spectrom.*, 2010, **292**, 48-52.
20. M. J. Ryding and E. Uggerud, *Phys. Chem. Chem. Phys.*, 2014, **16**, 9371-9382.
21. W. A. Pryor and G. L. Squadrito, *Am. J. Physiol.-Lung C.*, 1995, **268**, L699-L722.
22. P. Pacher, J. S. Beckman and L. Liaudet, *Physiol. Rev.*, 2007, **87**, 315-424.
23. I. M. Piskarev, I. P. Ivanova, S. V. Trofimova, A. A. Ichetkina and O. E. Burkhina, *High Energ. Chem.*, 2014, **48**, 350-352.
24. M. Manuszak and W. H. Koppenol, *Thermochim. Acta*, 1996, **273**, 11-15.
25. I. M. Piskarev, I. P. Ivanova, S. V. Trofimova, A. A. Ichetkina and O. E. Burkhina, *High Energ. Chem.*, 2014, **48**, 213-216.
26. C. H. Depuy and V. M. Bierbaum, *Accounts. Chem. Res.*, 1981, **14**, 146-153.
27. R. G. Keesee and A. W. Castleman, *J. Geophys. Res.-Atmos.*, 1985, **90**, 5885-5890.
28. A. A. Viggiano, *Mass Spectrom. Rev.*, 1993, **12**, 115-137.
29. D. Smith and P. Spanel, *Mass Spectrom. Rev.*, 1995, **14**, 255-278.
30. A. Luts and T. Parts, *J. Atmos. Sol.Terr. Phy.*, 2002, **64**, 763-774.
31. A. Hirsikko, T. Nieminen, S. Gagne, K. Lehtipalo, H. E. Manninen, M. Ehn, U. Horrak, V. M. Kerminen, L. Laakso, P. H. McMurry, A. Mirme, S. Mirme, T. Petaja, H. Tammet, V. Vakkari, M. Vana and M. Kulmala, *Atmos. Chem. Phys.*, 2011, **11**, 767-798.
32. F. L. Eisele, E. R. Lovejoy, E. Kosciuch, K. F. Moore, R. L. Mauldin, J. N. Smith, P. H.

McMurry and K. Iida, *J. Geophys. Res.-Atmos.*, 2006, **111**.
33. C. H. Depuy, V. M. Bierbaum, R. J. Schmitt and R. H. Shapiro, *J. Am. Chem. Soc.*, 1978, **100**, 2920-2921.
34. J. H. Bowie, C. H. Depuy, S. A. Sullivan and V. M. Bierbaum, *Can. J. Chem.*, 1986, **64**, 1046-1051.
35. P. U. Andersson, M. J. Ryding, O. Sekiguchi and E. Uggerud, *Phys. Chem. Chem. Phys.*, 2008, **10**, 6127-6134.
36. A. S. Zatula, P. U. Andersson, M. J. Ryding and E. Uggerud, *Phys. Chem. Chem. Phys.*, 2011, **13**, 13287-13294.
37. M. J. Ryding, A. S. Zatula, P. U. Andersson and E. Uggerud, *Phys. Chem. Chem. Phys.*, 2011, **13**, 1356-1367.
38. M. J. Ryding, A. M. Jonsson, A. S. Zatula, P. U. Andersson and E. Uggerud, *Atmos. Chem. Phys.*, 2012, **12**, 2809-2822.
39. M. J. Ryding, K. Ruusuvuori, P. U. Andersson, A. S. Zatula, M. J. McGrath, T. Kurtén, I. K. Ortega, H. Vehkamäki and E. Uggerud, *J. Phys. Chem. A*, 2012, **116**, 4902-4908.
40. J. E. Bartmess, in *NIST Chemistry WebBook, NIST Standard Reference Database*, eds. P. J. Linstrom and W. G. Mallard, National Institute of Standards and Technology, Gaithersburg MD, 20899. http://webbook.nist.gov (accessed 2015-12-12).
41. M. W. J. Chase, *J. Phys. Chem. Ref. Data*, 1998, **Monograph 9**, 1-1951.
42. T. M. Miller, in *CRC Handbook of Chemistry and physics, internet version 2006*, ed. D. R. Lide, Taylor and Francis, Boca Raton, FL, USA, 86th edn., 2006.
43. T. Su and M. T. Bowers, *Int. J. Mass Spectrom. Ion Phys.*, 1973, **12**, 347-356.
44. G. Kummerlowe and M. K. Beyer, *Int. J. Mass Spectrom.*, 2005, **244**, 84-90.
45. T. Su and M. T. Bowers, *J. Chem. Phys.*, 1973, **58**, 3027-3037.
46. G. Gioumousis and D. P. Stevenson, *J. Chem. Phys.*, 1958, **29**, 294-299.
47. T. M. Miller, in *CRC Handbook of Chemistry and physics, internet version 2006*, ed. D. R. Lide, Taylor and Francis, Boca Raton, FL, USA, 86th edn., 2006.
48. "Dipole Moments" in *CRC Handbook of Chemistry and physics, internet version 2006*, ed. D. R. Lide, Taylor and Francis, Boca Raton, FL, USA, 86th edn., 2006.
49. J. A. Rutherford and B. R. Turner, *J. Geophys. Res.*, 1967, **72**, 3795-3800.
50. A. R. Hoy, J. W. C. Johns and A. R. W. McKellar, *Can. J. Phys.*, 1975, **53**, 2029-2039.
51. A. Gijsbertsen, W. Siu, M. F. Kling, P. Johnsson, P. Jansen, S. Stolte and M. J. J. Vrakking, *Phys. Rev. Lett.*, 2007, **99**, 213003.
52. S. Green, *Chem. Phys. Lett.*, 1973, **23**, 115-119.
53. R. Sayos, R. Valero, J. M. Anglada and M. Gonzalez, *J. Chem. Phys.*, 2000, **112**, 6608-6624.
54. F. P. Billingsley, *J. Chem. Phys.*, 1975, **62**, 864-874.
55. S. R. Langhoff, C. W. Bauschlicher and H. Partridge, *Chem. Phys. Lett.*, 1994, **223**, 416-422.
56. S. G. Lias and M. M. Meot-Ner, in *NIST Chemistry WebBook, NIST Standard Reference Database*, eds. P. J. Linstrom and W. G. Mallard, National Institute of Standards and Technology, Gaithersburg MD, 20899. http://webbook.nist.gov (accessed 2015-12-12).
57. D. J. Anick, *J. Phys. Chem. A*, 2011, **115**, 6327-6338.
58. M. M. Meot-Ner and S. G. Lias, in *NIST Chemistry WebBook, NIST Standard Reference Database*, eds. P. J. Linstrom and W. G. Mallard, National Institute of Standards and Technology, Gaithersburg MD, 20899. http://webbook.nist.gov (accessed 2015-12-12).
59. D. L. Thomsen, J. N. Reece, C. M. Nichols, S. Hammerum and V. M. Bierbaum, *J. Am. Chem. Soc.*, 2013, **135**, 15508-15514.
60. M. J. Ryding, A. Debnarova, I. Fernandez and E. Uggerud, *J. Org. Chem.*, 2015, **80**, 6133-6142.
61. R. Kissner, T. Nauser, C. Kurz and W. H. Koppenol, *IUBMB Life*, 2003, **55**, 567-572.
62. T. Logager and K. Sehested, *J. Phys. Chem.*, 1993, **97**, 6664-6669.

63. D. A. Dixon, D. Feller, C. G. Zhan and J. S. Francisco, *J. Phys. Chem. A*, 2002, **106**, 3191-3196.
64. I. M. Konen, I. B. Pollack, E. X. J. Li, M. I. Lester, M. E. Varner and J. F. Stanton, *J. Chem. Phys.*, 2005, **122**, 094320.
65. D. M. Golden, J. R. Barker and L. L. Lohr, *J. Phys. Chem. A*, 2003, **107**, 11057-11071.
66. M. J. Frisch, G. W. Trucks, H. B. Schlegel, G. E. Scuseria, M. A. Robb, J. R. Cheeseman, G. Scalmani, V. Barone, B. Mennucci, G. A. Petersson, H. Nakatsuji, M. Caricato, X. Li, H. P. Hratchian, A. F. Izmaylov, J. Bloino, G. Zheng, J. L. Sonnenberg, M. Hada, M. Ehara, K. Toyota, R. Fukuda, J. Hasegawa, M. Ishida, T. Nakajima, Y. Honda, O. Kitao, H. Nakai, T. Vreven, J. J. A. Montgomery, J. E. Peralta, F. Ogliaro, M. Bearpark, J. J. Heyd, E. Brothers, K. N. Kudin, V. N. Staroverov, R. Kobayashi, J. Normand, K. Raghavachari, A. Rendell, J. C. Burant, S. S. Iyengar, J. Tomasi, M. Cossi, N. Rega, J. M. Millam, M. Klene, J. E. Knox, J. B. Cross, V. Bakken, C. Adamo, J. Jaramillo, R. Gomperts, R. E. Stratmann, O. Yazyev, A. J. Austin, R. Cammi, C. Pomelli, J. W. Ochterski, R. L. Martin, K. Morokuma, V. G. Zakrzewski, G. A. Voth, P. Salvador, J. J. Dannenberg, S. Dapprich, A. D. Daniels, O. Farkas, J. B. Foresman, J. V. Ortiz, J. Cioslowski and D. J. Fox, *Gaussian 09*, (2009) Gaussian, Inc., Wallingford, CT, USA.
67. Y. Zhao and D. G. Truhlar, *Accounts. Chem. Res.*, 2008, **41**, 157-167.
68. L. A. Curtiss, P. C. Redfern and K. Raghavachari, *J. Chem. Phys.*, 2007, **126**, 084108.
69. J. W. Mciver and Komornic.A, *J. Am. Chem. Soc.*, 1972, **94**, 2625-2633.
70. C. Gonzalez and H. B. Schlegel, *J. Phys. Chem.*, 1990, **94**, 5523-5527.